RSC Advances

PAPER

View Article Online
View Journal | View Issue

Cite this: *RSC Adv.*, 2021, **11**, 12349

Efficient one-pot synthesis and dehydrogenation of tricyclic dihydropyrimidines catalyzed by OMS-2-SO_3H, and application of the functional-chromophore products as colorimetric chemosensors†

Neda Mardazad, Alireza Khorshidi * and Abdollah Fallah Shojaei

An efficient and convenient one-pot multicomponent reaction (MCR) for the synthesis and dehydrogenation of tricyclic dihydropyrimidine derivatives, catalyzed by $-SO_3H$ functionalized octahedral manganese oxide molecular sieves (OMS-2-SO_3H) as a novel solid acid catalyst, is reported. All of the organic products and the catalyst were unambiguously characterized with conventional techniques including Fourier-transform infrared spectroscopy (FT-IR), scanning electron microscopy (SEM), high-resolution transmission electron microscopy (HRTEM), X-ray diffraction analysis (XRD), ^{1}H NMR, and ^{13}C NMR spectroscopy. The targeted dehydrogenated chromophore compounds were successfully used as colorimetric chemosensors for detection of transition metals in aqueous solution. For example, 1-[4-(4-hydroxy-3-methoxy-phenyl)-2-methyl-benzo[4,5]imidazo[1,2-*a*]pyrimidin-3-yl]-ethanone (**7d**), exhibited high sensitivity and selectivity toward detection of Cr^{3+} over a panel of other transition metal cations. The interference of foreign ions was found to be negligible. It was found that a 1 : 1 complex of Cr^{3+} and **7d** is responsible for the color change of the solution from ochre to brown. These newly devised chemosensors can also exhibit significant wavelength shifts (up to 100 nm) when used as pH indicators. **7d** for example, showed a vivid and sharp color change from pink to yellow in the pH range of 4 to 6.

Received 6th February 2021
Accepted 23rd March 2021

DOI: 10.1039/d1ra01005k

rsc.li/rsc-advances

Introduction

The design and development of chemosensors have expanded substantially in last few decades. Design and synthesis of new chemosensors for d-metal ions, *i.e.* transition metals including heavy metal ions, have been of great interest for chemists in recent years as they play important roles in the areas of chemical,[1,2] biological,[3,4] and environmental systems.[5,6] Among the chemosensors, the naked eye ones, *i.e.* the colorimetric chemosensors, are most significant because they don't involve either any costly instrument or pre-treatment of the sample,[7–12] *i.e.*, analyte.

We live in a toxic globe. Every day we are exposed to several toxic metallic species and chemicals, food additives, pesticides, industrial wastes, *etc.* The term "hazardous metal" has been used as a general term for those metals which possess potential toxicity against human and/or environment.[13] In spite of having toxic effects, some d-metal ions are beneficial also, particularly in small quantities (trace metals) and are nutritionally indispensable for a healthy life.

Among the metal ions, Cr^{3+} ion performs a crucial role in a wide range of biochemical processes, which is essential for good health in moderate intake. However, it is toxic at high concentrations.[14–16]

For a stable human or animal diet, intake amount of 50–200 μg of Cr^{3+} is necessary. However, the presence of Cr^{3+} in excess amount deteriorates the environment and can also spoil the cellular structures.[17,18] The mechanism by which Cr^{3+} affects human metabolism is based on modulation of the action of insulin through glucose tolerance factors (GTF), thereby activating certain enzymes and stabilizing proteins and nucleic acids. A deficiency of chromium in the human body would lead to a variety of diseases, including diabetes and cardiovascular disease. Recently, Cr(III) has also been shown to adversely affect cellular structures, although it's *in vivo* toxicity observed is much lower than that of Cr(VI).[19,20] Several biological functions depend directly or indirectly on the proper concentration and oxidation states of chromium to maintain the homoeostatic mechanism. Deficiency or overdose of chromium can lead to

Department of Chemistry, Faculty of Sciences, University of Guilan, 41335-1914, Rasht, Iran. E-mail: khorshidi@guilan.ac.ir; Fax: +9801333367262; Tel: +989113397159

† Electronic supplementary information (ESI) available: X-ray diffraction patterns, FTIR, ^{1}H NMR, and ^{13}C NMR spectra of all of the synthesized materials. See DOI: 10.1039/d1ra01005k

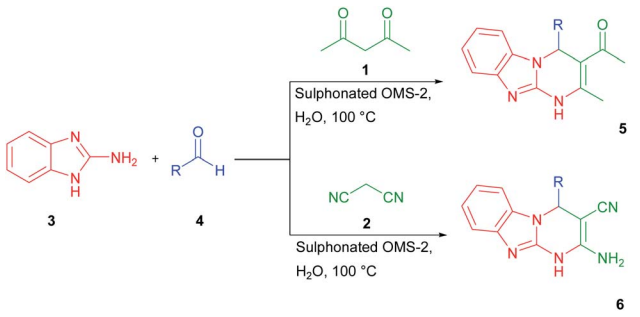

Scheme 1 Synthesis of benzo[4,5]imidazo[1,2-*a*]pyrimidines (**5**) and 2-amino-4-substituted-1,4-dihydrobenzo[4,5]imidazole (**6**).

serious diseases, including Alzheimer's, Huntington's and Parkinson's disease.[21,22]

It is clear that the rational design and synthesis of efficient chemosensors for the selective detection of d-metal ions is of great importance for the purpose of public health and environment. Here we report a simple and easy to make imidazole-based chemosensor for Cr^{3+} based on the proton transfer signalling mode. Chromophores are functional π-electron systems that lay the molecular foundation of modern organic electronics and solar energy conversion with tailored small molecules.[23] Hence, the efficient and rapid preparation of these novel functional organic molecules with specific photophysical and electrochemical properties remains an ultimate goal and challenge for researchers both in organic chemistry and materials science. In particular, multicomponent processes exactly tackle these synthetic challenges and, therefore, they have received considerable interest both in academia and industry, predominantly for synthesizing biologically active molecules.[24–27] By definition, multicomponent reactions (MCRs) are a type of convergent organic reactions in which three or more precursors react in a one-pot fashion without isolation and purification of intermediates. These reactions have demonstrated a remarkable impact on the synthesis of complex products, with high atom economy and molecular diversity. In addition, the MCRs are straightforward for the synthesis of compounds with biological or pharmacological properties which is highly attractive for the pharmaceutical and agrochemical industries, among others.[28,29] In the past decades, several MCRs have been well developed and widely used in natural product synthesis and drug discovery.[30–32] Therefore, the development of MCRs for construction of biologically interesting molecules continues to attract considerable attention for their obvious atom- and step-economy. The multifunctionalized dihydropyrimidine scaffold (DHPMs) represents a heterocyclic system of remarkable pharmacological efficiency. In the past decades, a broad range of biological effects, including antiviral, antitumor, antibacterial, and anti-inflammatory activities, has been ascribed to these partly reduced pyrimidine derivatives.[33] Dihydropyrimidines, the products of the Biginelli reaction, are widely used in the pharmaceutics as calcium channel blockers, antihypertensive agents, and alpha-1-a-antagonists.[34–36] It has been suggested that the substituent effect can be attributed to intramolecular hydrogen bonding between the–alkoxy oxygen and the proton of the pyrimidine ring NH moiety.[37]

Among dihydropyrimidine derivatives, the benzo[4,5]imidazo[1,2-*a*]-pyrimidines have been reported to have a variety of biological activities, such as antineoplastic activity,[38] protein kinase inhibitory,[39] T cell activation,[40] TIE-2 and/or VEGFR2 inhibitory activities.[41]

The known methods of the synthesis of benzo[4,5]imidazo [1,2-*a*]-pyrimidines suffer from some drawbacks including low yield, prolonged reaction time, and consumption of organic solvents. So, there is an urgent need to develop an alternative protocol for efficient and convenient MCRs synthesis of this type of heterocyclic compounds (Scheme 1).

Porous manganese oxide natural materials, on the other hand, are found as manganese nodules, and when dredged from the ocean floors have been used as excellent adsorbents of metals, for example from electroplating wastes, and have been shown to have excellent catalytic activity.[42–44] Variable pore size materials have been synthesized using structure directors by a variety of synthetic methodologies. Catalytic performance of these OMS materials have been shown to be related to the redox cycling of various oxidations states of manganese such as Mn^{2+},

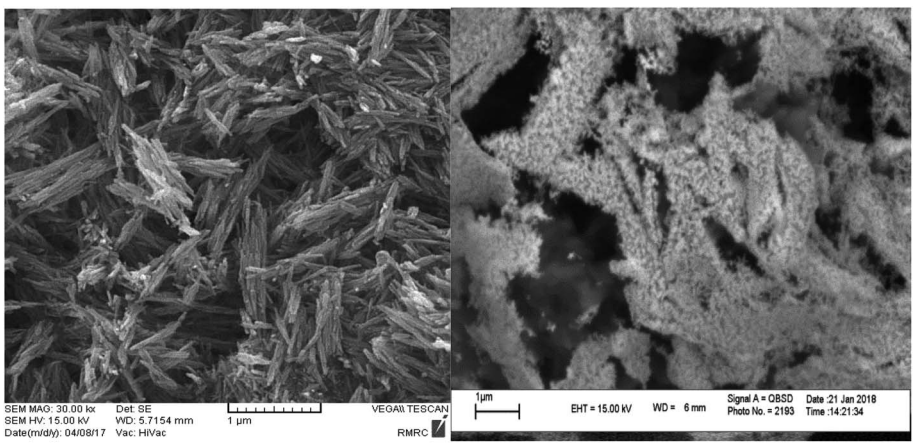

Fig. 1 SEM micrograph images of the synthesized OMS-2 (left) and sulfonated OMS-2 (right).

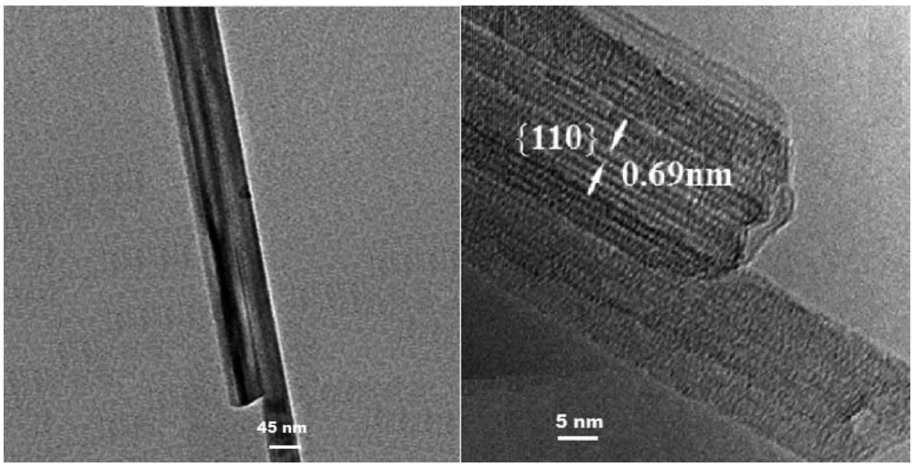

Fig. 2 High-resolution transmission electron microscope (HRTEM) images of OMS-2-SO_3H.

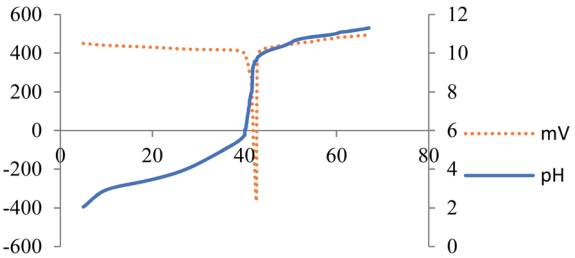

Fig. 3 Potentiometric titration curve of the OMS-2-SO_3H (0.1 N NaOH as titrant).

Mn^{3+}, and Mn^{4+}.[45] Many concepts including nonstoichiometry, defects, oxygen vacancies, and intermediates are fundamental to many of the syntheses, characterization, and applications such as fuel cells, adsorption, sensors, batteries, and so on.[46–48] A key phase that shows outstanding electrochemical and catalytic properties is the 2 × 2 synthetic cryptomelane or OMS-2 structure.[49–51]

In this contribution, we report the first modification of OMS-2 with chlorosulfonic acid to form –SO_3H functionalized OMS-2 (OMS-2-SO_3H). The idea was inspired by the excellent performance of solid acid catalysts based on –SO_3H functionalized silica materials as heterogeneous catalysts.[52–54]

Results and discussion

Catalyst characterization

Sulfonated OMS-2 was subjected to XRD analysis to identify its crystal structure and crystallinity after sulfonation. Fig. S1† shows the XRD patterns for the OMS-2 and its sulfonated form. The observed reflections at 2θ values of 12°, 17.8°, 28.5°, 37.4°, 41.6°, 49.7°, 56°, 59.9°, 65.2°, and 69.3° can be indexed to the 110, 200, 310, 211, 301, 411, 600, 521, 602, and 541 planes of Q-phase cryptomelane-type manganese oxide (JCPDS card no. 29-

Table 1 Condensation of 2-aminobenzimidazole (**3**), 9-anthracenecarboxaldehyde (**4a**), and acetylacetone (**1**) in presence of OMS-2-SO_3H[a]

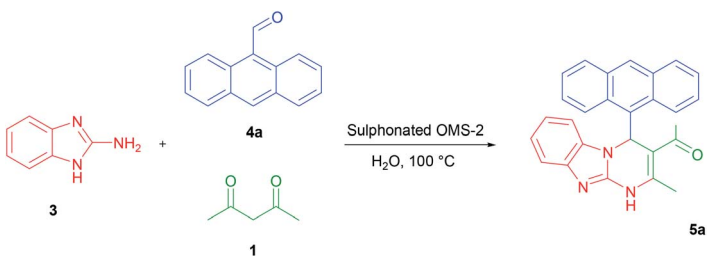

Entry	Catalyst (mol%)	Time (h)	Yield of **5a**[b] (%)
1	0	4	20
2	5	1	75
3	10	1	96
4	20	1	96

[a] Conditions: 2-aminobenzimidazole **3** (2 mmol), 9-anthracenecarboxaldehyde **4a** (2 mmol), and ethyl acetoacetate **1** (2 mmol), H_2O (2 mL) at 100 °C. [b] Isolated yields.

Table 2 Condensation of 2-aminobenzimidazole (**3**), 9-anthracenecarboxaldehyde (**4a**), and acetylacetone (**1**) in different solvents[a]

Entry	Solvent	Temp. (°C)	Time (h)	Yield of **5a**[b] (%)
1	THF	100	4	30
2	Toluene	100	4	50
3	MeCN	100	4	60
4	DCM	100	4	30
5	DMF	100	4	45
6	EtOH	100	1	88
7	H_2O	100	1	96
8	H_2O	40	7	20
9	H_2O	60	6	50
10	H_2O	80	4	65

[a] Conditions: 2-aminobenzimidazole **3** (2 mmol), 9-anthracenecarboxaldehyde **4a** (2 mmol), acetylacetone **1** (2 mmol), OMS-2-SO_3H (0.1 mmol, 10 mol%), solvent (2 mL). [b] Isolated yields.

1020) for both samples. To study the morphological changes of OMS-2 after sulfonation, electron microscopy imaging (SEM) was used (Fig. 1). SEM micrographs revealed a rod-shaped morphology for the OMS-2 sample, as anticipated. After sulfonation, however, surface of the nano-rods became rough and non-porous. High-resolution transmission electron microscope (HRTEM) imaging (Fig. 2), on the other hand, showed that OMS-2-SO_3H is consisted of almost uniform nano-rods of about 45 nm in diameter. Fig. 2, right, shows that the fibres lie on the (110) plane. One can also note that the lattice fringes are separated by 0.69 nm. These findings are in agreement with the reported characteristics of the parent OMS-2.

Nitrogen adsorption–desorption (BET) analysis showed that the specific surface area of the catalyst was changed from 93 m^2 g^{-1} to 202.21 m^2 g^{-1}. This increase in the surface area is in agreement with the SEM observations, and is in line with the previous reports.[55] It should be noted that the sulfonated sample was highly hygroscopic, and its high hydrophilicity may result in formation of a layer of water on its surface.

To further characterize the synthesized samples, FT-IR spectroscopy was used (Fig. S2†). In the FT-IR spectrum of OMS-2-SO_3H, the observed peaks can be attributed as follows: stretching and bending vibrations of the adsorbed water: 3415 and 1635 cm^{-1}; symmetric and asymmetric stretching vibration of S=O: 1286 and 1178 cm^{-1}; stretching vibration of S=O: 1067 cm^{-1}; C–S stretching vibrations: 695 cm^{-1}; MnO_6 vibrations: 735, 594 and 535 cm^{-1}. It is also evident that the intensity of the peak at about 3400 cm^{-1} has been increased, which is a direct indication of the inclusion of –SO_3H functionality.

Acidity determination

Quantification of the acidity of the OMS-2-SO_3H was achieved by potentiometric titration with 0.1 N NaOH. The corresponding titration curve is depicted in Fig. 3. The acidity was found to be 119.66 mmol –SO_3H per g of the solid acid catalyst.

Optimization of the reaction conditions

Initially, we studied the three-component condensation reaction of 2-aminobenzimidazole **3** (2 mmol), 9-anthracenecarboxaldehyde **4a** (2 mmol), and acetylacetone **1** (2 mmol) in presence of OMS-2-SO_3H (10 mol%) in 2 mL H_2O at 100 °C for 1 h to give the desired product **5a** in 96% yield. However, only 20% yield of the target product **5a** was observed when the mixture was stirred under similar conditions in the absence of the catalyst even after 4 h (Table 1, entry 1). Encouraged by the result, we further investigated the best reaction conditions by using different amounts of OMS-2-SO_3H. An increase in the quantity of the catalyst from 0 mol% to 10 mol%, not only decreased the reaction time from 4 h to 1 h, but also increased the product yield from 20% to 96% (Table 1, entries 1–3). However, the yield did not increase when excess amount (20 mol%) of the catalyst was used under the same conditions. Therefore, 10 mol% of the OMS-2-SO_3H was considered as the optimized amount of the catalyst.

As shown in Table 2, solvent had an impact on the yield of the target product **5a** (30–50%). The obtained yields in THF, DCM, toluene, and DMF (Table 2, entries 1, 2, 4 and 5) were indicative of the effect of the solvent nature on the reaction. Obviously, protic solvents such as EtOH and H_2O resulted in better yields (88 and 96%, Table 2, entries 6 and 7). Thus, H_2O was selected as the solvent for all of the subsequent reactions. Furthermore, in order to optimize the reaction temperature, the target multicomponent reaction was carried out in the range of 40–100 °C (Table 2, entries 7–10). It was found that elevated temperature had a significant effect on the reaction yield.

Table 3 Synthesis of benzo[4,5]imidazo[1,2-*a*]pyrimidines (**5**) and 2-amino-4-substituted-1,4-dihydrobenzo[4,5]imidazolo[1,2-*a*]pyrimidine-3-carbonitriles (**6**) catalyzed by OMS-2-SO_3H[a]

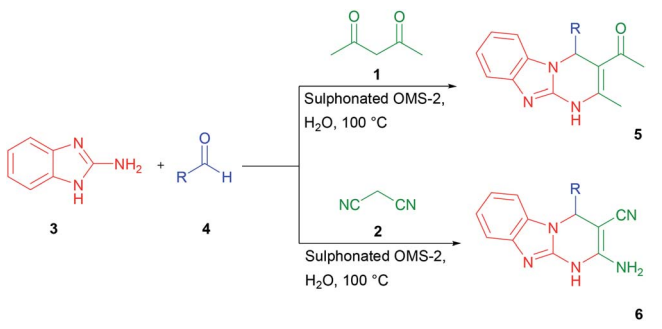

Entry	**1** or **2**[b]	R	Product	Time (min)	Yield[c] (%)
1	**1**	Anthracen-9-yl	**5a**	45	96
2	**1**	2-$NO_2C_6H_4$	**5b**	90	84
3	**1**	5-Br-2-OHC_6H_3	**5c**	60	89
4	**1**	4-OH-3-$CH_3OC_6H_3$	**5d**	60	88
5	**2**	Anthracen-9-yl	**6a**	30	90
6	**2**	2-$NO_2C_6H_4$	**6b**	30	87
7	**2**	5-Br-2-OHC_6H_3	**6c**	20	94
8	**2**	4-OH-3-$CH_3OC_6H_3$	**6d**	10	94

[a] Conditions: 2-aminobenzimidazole **3** (2 mmol), aldehyde **4** (2 mmol), and acetylacetone **1** (2 mmol) or malononitrile **2** (2 mmol), OMS-2-SO_3H (0.1 mmol, 10 mol%), H_2O (2 mL) at 100 °C. [b] Acetylacetone (**1**) and malononitrile (**2**). [c] Isolated yields.

To examine the generality and scope of this OMS-2-SO_3H catalyzed reaction, we used a series of aldehydes in the title reaction (Table 3). In all cases, the substrates reacted smoothly to give the corresponding benzo[4,5]imidazo[1,2-*a*]pyrimidines and 2-amino-4-substituted-1,4-dihydrobenzo[4,5]imidazolo[1,2-*a*]pyrimidine-3-carbonitriles in good yields (Table 3, entries 1–8). Most importantly, aromatic aldehydes carrying either electron-donating or electron-withdrawing substituents could react efficiently to give the desired products without significant differences. The reaction was tolerant to a variety of functional groups, such as $-OCH_3$, –OH, $-NO_2$, and Br.

Tricyclic dihydropyrimidine derivatives containing an H atom in the *meso* position were expected to be able to easily oxidize to the corresponding conjugated products. It was also expected that the resulting conjugated compounds might display interesting transition metal cation binding and sensing properties. The choice of oxidized form of tricyclic dihydropyrimidine derivatives as the chromogenic-sensing molecule was mainly based on the fact that this conjugated skeleton could act not only as a color-reporting group but also as a binding affinity control group containing an acidic H-bond donor moiety and a basic H-bond acceptor moiety. Interestingly, after a series of optimization experiments, a one-pot method was devised for the synthesis and *in situ* oxidation of benzo[4,5]imidazo[1,2-*a*]pyrimidines (**5**) and 2-amino-4-substituted-1,4-dihydrobenzo[4,5]imidazolo[1,2-*a*]pyrimidine-3-carbonitriles (**6**) to the corresponding dehydrogenated products (**7** and **8**). The optimized conditions are summarized in Table 4.

As a representative example, the synthesis of **7d** is shown in Scheme 2. The oxidized product **7d** was prepared in 80% yield by condensation of 2-aminobenzimidazole **3**, 4-hydroxy-3-methoxybenzaldehyde **4d**, and acetylacetone **1** with DDQ in CH_3CN.

According to the obtained results, a plausible mechanism for the synthesis of dihydropyrimidine derivatives **5a–d** and **6a–d** catalyzed by the OMS-2-SO_3H is outlined in Scheme 3. At the first step, aldehydes **4** can be activated by the OMS-2-SO_3H solid acid, mainly through $-SO_3H$ groups, to afford the Knoevenagel condensation product of aldehydes **4** and acetylacetone (**1**) or malononitrile (**2**) C–H acid as intermediates (**II**) or (**II′**), respectively. Then, condensation of these intermediates with 2-

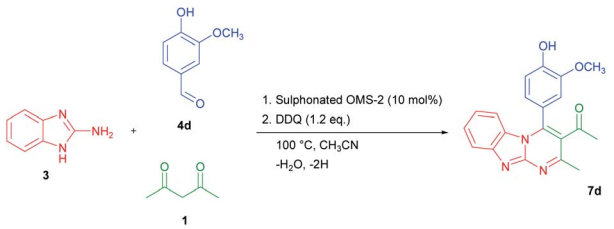

Scheme 2 Synthesis of 1-[4-(4-hydroxy-3-methoxy-phenyl)-2-methyl-benzo[4,5]imidazo[1,2-*a*]pyrimidin-3-yl]-ethanone (**7d**).

Table 4 One-pot synthesis and oxidation of benzo[4,5]imidazo[1,2-*a*]pyrimidines (**5**) and 2-amino-4-substituted-1,4-dihydrobenzo[4,5]imidazolo[1,2-*a*]pyrimidine-3-carbonitriles (**6**) to conjugated chromophores catalyzed by OMS-2-SO_3H[a]

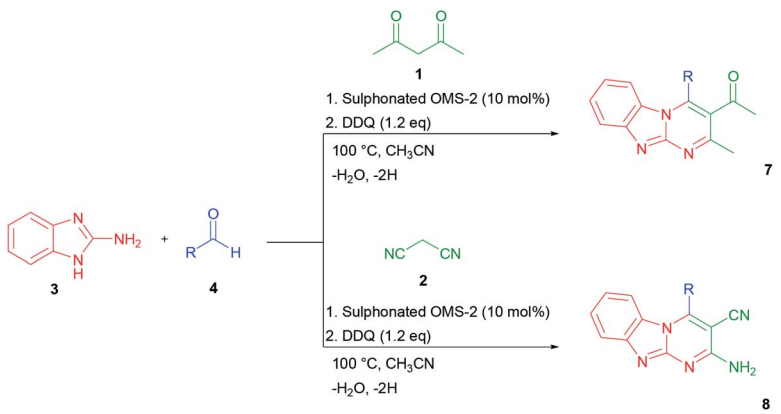

Entry	**1** or **2**[b]	R	Product	Time (min)	Yield[c] (%)
1	**1**	Anthracen-9-yl	**7a**	140	78
2	**1**	2-$NO_2C_6H_4$	**7b**	150	75
3	**1**	5-Br-2-OHC_6H_3	**7c**	150	68
4	**1**	4-OH-3-$CH_3OC_6H_3$	**7d**	120	80
5	**2**	Anthracen-9-yl	**8a**	110	72
6	**2**	2-$NO_2C_6H_4$	**8b**	110	65
7	**2**	5-Br-2-OHC_6H_3	**8c**	100	77
8	**2**	4-OH-3-$CH_3OC_6H_3$	**8d**	90	69

[a] Conditions: 2-aminobenzimidazole **3** (2 mmol), aldehyde **4** (2 mmol), and acetylacetone **1** (2 mmol) or malononitrile **2** (2 mmol), OMS-2-SO_3H (0.1 mmol, 10 mol%), DDQ (1.2 eq.), H_2O (2 mL) at 100 °C. [b] Acetylacetone (**1**) and malononitrile (**2**). [c] Isolated yields.

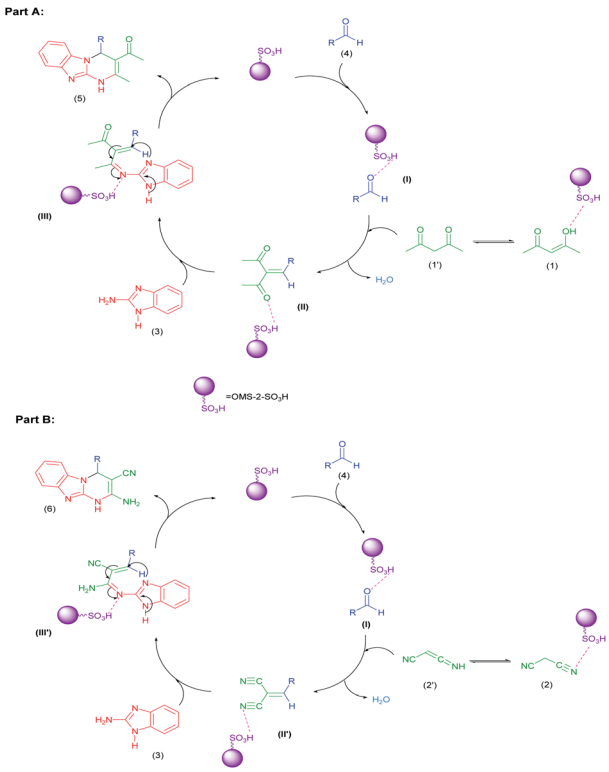

Scheme 3 A plausible mechanism for the synthesis of dihydropyrimidine derivatives **5a–d** (Part A) and **6a–d** (Part B) in the presence of the OMS-2-SO_3H catalyst.

aminobenzimidazole (**3**) produces Michael acceptor intermediates (**III**) or (**III′**), respectively, in the presence of OMS-2-SO_3H. Finally, the activated intermediates (**III**) or (**III′**) are involved in the intramolecular Michael addition and subsequent tautomerization to afford tricyclic dihydropyrimidine derivatives **5a–d** and **6a–d**, respectively.

To demonstrate the effectiveness of OMS-2-SO_3H, it was compared with some of the previously reported and published procedures (Table 5). The results clearly illustrate the superiority of this protocol against many of the others in terms of the product yield, reaction time and using a green solvent.

To study the properties of the synthesized products, their behaviour as a potential pH indicator was evaluated. Many dyes have been used as pH indicators due to the reversible

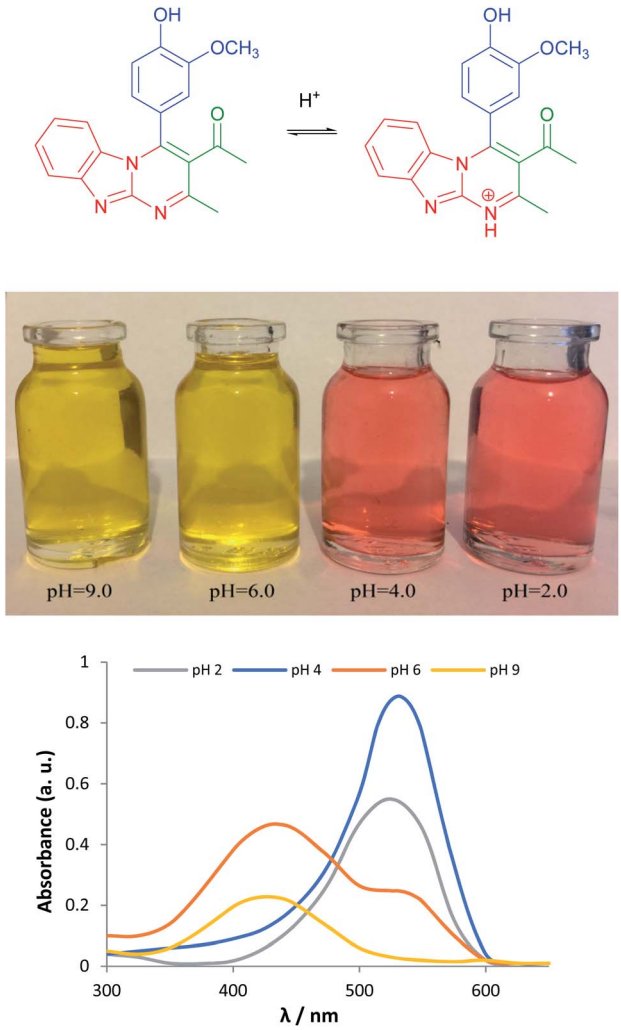

Fig. 4 (Top) and (middle) pH indication using **7d**, (bottom) spectral changes of **7d** (5×10^{-6} M, EtOH 70%) at different pH.

protonation–deprotonation processes. It was found that our synthesized products could act as pH indicators in the pH range of 4 to 6 with an extremely sharp and clear colour change. The colour changes during this pH range are attributed to an intramolecular charge transfer mechanism resulting from the

Table 5 The comparison of the catalytic efficiency of OMS-2-SO_3H

Entry	Catalyst	Conditions	Time (min)	Yield (%)	Ref.
1	$KAl(SO_4)_2 \cdot 12H_2O$	Ethanol, reflux	210	86	56
2	*p*-TSA	Solvent-free, 80 °C	30	93	57
3	Triethylamine	Ethanol, reflux	180	60	58
4	MgO	CH_3CN, reflux	45	75	59
5	Thiamine hydrochloride (VB1)	H_2O, reflux	180	90	60
6	SBA-IL	Solvent-free, 150 °C	40	87	61
7	TBBDA	Solvent-free, 100 °C	80	88	62
8	H_3PO_4–Al_2O_3	Solvent-free, 100 °C	85	90	63
9	Sulfamic acid	Solvent-free, 85 °C	480	88	64
10	OMS-2-SO_3H	H_2O, 100 °C	45	96	This work

Table 6 Position of **7a–d** and **8a–d** as indicators among commonly used pH indicators in the pH range of 4–6

Transition range, pH	Indicator	Colour change	Composition of indicator's solution, %
4.0–6.0	Dyes **7a–d**, **8a–d**	Pink-yellow	0.1 (in 70% ethanol)
4.3–6.3	Alizarin (red) S	Yellow-pink	0.1 (in water)
4.4–6.2	Methyl red	Red-yellow-orange	0.1 (in 96% ethanol)
4.5–6.2	Methyl red sodium salt	Red-yellow-orange	0.05 (in water)
4.7–6.3	Bromophenol red	Yellow-purple	0.1 (in 20% ethanol)
4.8–6.4	Chlorophenol red	Yellow-purple	0.1 (in 20% ethanol)

push–pull effect of the electron-donating amine substituent. The colour transition of compound **7d** is depicted in Fig. 4.

Table 6 compares the transition range of our products with other pH indicators in the pH range 4–6.[65]

From the data listed in Table 6, it is clear that the synthesized dyes exhibited quite acceptable properties to be used as indicators. A dilute solution of **7d** (5×10^{-6} M, EtOH 70%), presented a pink colour and displayed a strong absorption band at 430 nm, which may be attributable to the intramolecular charge transfer (ICT) arising from the π-extended conjugated structure of this compound. Upon addition of dilute acid (0.1 M HCl) to this solution, however, the absorption band was red-shifted to higher wavelengths around 530 nm, along with a distinctive colour change to yellow. Fig. 4 shows the spectroscopic behaviour of **7d** at different pH.

To determine the colour transition range of the indicator, absorption of the solution was measured at 531 nm with gradual addition of dilute alkali solution (NH_4OH). The result is shown in Fig. 5. As is apparent, a sharp colour transition was observed in the pH range of 4.0–6.0, which is comparable to methyl red.

Encouraged by these results, we decided to study the ability of our products in sensing transition metal cations. It was found that these dehydrogenated chromophore compounds interact with transition metal cations resulting to distinct spectral changes. For example, compound **7d** exhibited hypsochromic effects in presence of some metal cations including Ca^{2+}, Cr^{3+}, Co^{2+} and Cu^{2+}. The most intense colour change was observed for Cr^{3+} in acetonitrile solution. This result indicates that **7d** can serve as a 'naked eye' Cr^{3+} indicator. The UV-vis spectrum of **7d** (5×10^{-6} M) and Cr^{3+} (1.25×10^{-4} M) solutions in CH_3CN, before and after mixing, is shown in Fig. 6.

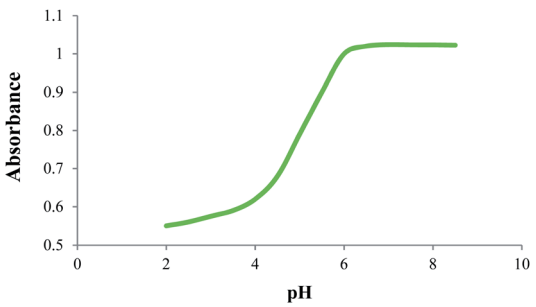

Fig. 5 Determination of the color transition range of **7d**: λ_{max} 531.

As shown in Fig. 6, Cr^{3+} shows classic transitions of a d^3 cation corresponding to transitions from the $^4A_{2\ (F)}$ ground state to the $^4T_{1\ (F)}$ and $^4T_{1\ (P)}$ excited states of the metal cation. After mixing **7d** and Cr^{3+} solutions, a blue shift of about 40 nm for the 420 nm band of **7d** was observed that might be due to N-bonding of **7d** to the metal centre.

The spectral response of **7d** to other transition metal cations (Ca^{2+}, Fe^{3+}, Ni^{2+}, Cr^{3+}, Co^{2+}, Cu^{2+}, Zn^{2+}, Cd^{2+}, Mn^{2+}, Hg^{2+} and Sn^{2+}) are depicted in Fig. 7.

In Fig. 8 effect of foreign metal ions on the fluorescence intensity of the **7d** + Cr^{3+} system is presented. There was almost no interference for the detection of Cr^{3+} in the presence of alkali and alkaline earth metal ions (Na^+, K^+, Mg^{2+}, Ca^{2+}), and several other transition metal ions (Mn^{2+}, Fe^{3+}, Co^{3+}, Ni^{2+}, Cu^{2+}, Zn^{2+},

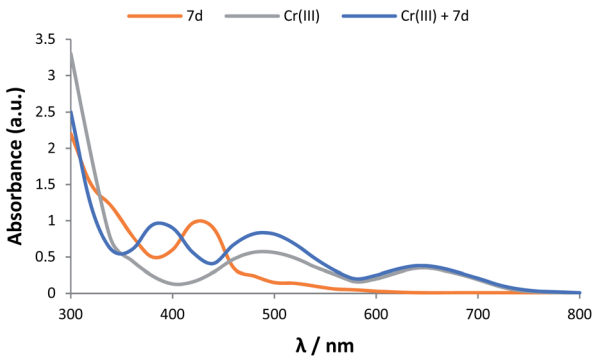

Fig. 6 UV-vis spectra of **7d** (5×10^6 M), Cr^{3+} (1.25×10^4 M), and a 1 : 1 mixture of **7d** and Cr^{3+} solutions in acetonitrile.

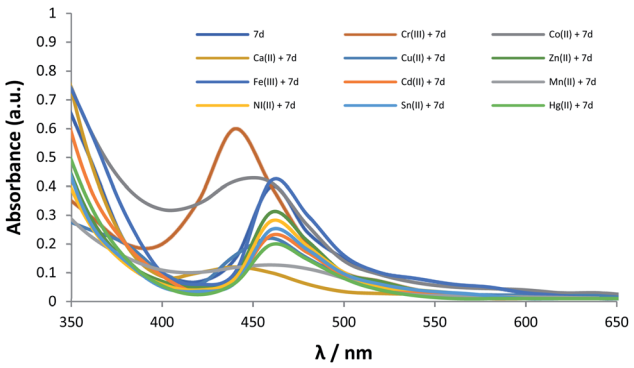

Fig. 7 The spectral response of **7d** to other transition metal cations (Ca^{2+}, Fe^{3+}, Ni^{2+}, Cr^{3+}, Co^{2+}, Cu^{2+}, Zn^{2+}, Cd^{2+}, Mn^{2+}, Hg^{2+} and Sn^{2+}).

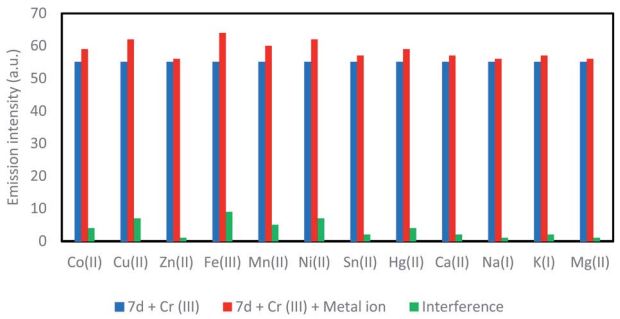

Fig. 8 Interference of foreign cations. [blue: **7d** + Cr^{3+}; red: **7d** + Cr^{3+} + other metal ion; green: resulting interference].

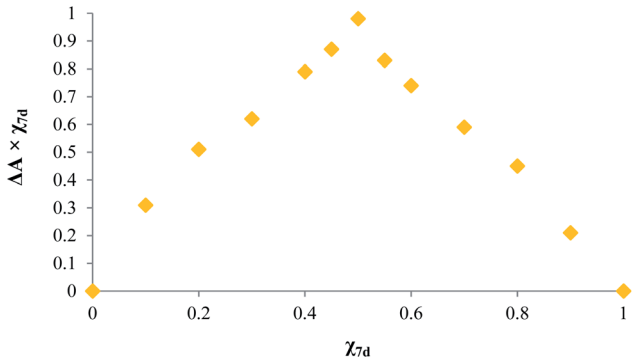

Fig. 9 A Job plot for the complexation of **7d** with Cr^{3+} indicating the formation of a 1 : 1 complex.

Sn^{2+}, Hg^{2+}). In this study, **7d** = 10^{-6} mol L^{-1}, [Cr^{3+}] = 10^{-6} mol L^{-1} and the foreign metal ions are present 10 times of the [Cr^{3+}] *i.e.* 10^{-5} mol L^{-1}. All these observations indicate that **7d** exhibits a highly preferential binding of Cr^{3+} over other metal ions. The combined results revealed that **7d** can be used to detect Cr^{3+} without interference from other metal ions, and is a good chemosensor for detection of Cr^{3+}.

In order to gain an insight into the interaction mechanism between the cation and the receptors, a similar experiment with Cr^{3+} was conducted in acetonitrile at acidic pH (pH 2.0). In this case, the blue-shifted band was not observed upon addition of the metal, revealing that no interaction took place due to the fact that the imidazole moiety of **7d** was N-protonated. A 1 : 1 stoichiometry of the complex as indicated by the changes in the colorimetric response of **7d**, in the presence of the varying concentrations of Cr^{3+} (Fig. 9), is also in agreement with N-coordination of the metal.

Conclusions

In summary, a series of newly oxidized tricyclic dihydropyrimidine derivatives were synthesized one-pot, under heterogeneous catalysis of OMS-2-SO_3H as a newly devised solid acid catalyst. The organic products were used as colorimetric probes for the detection of transition metal ions in aqueous solution. Formation of 1 : 1 complexes of the chemosensor and cation was found to be responsible for the observed colour changes. The excellent selectivity of the synthesized chemosensors may provide a suitable platform for application in biological monitoring, for example, in tracking of Cr^{3+}. The obtained dehydrogenated dihydropyrimidines were also capable to be used as pH indicators based on the proton transfer signaling mode. The outcome of our research is expected to pave the way for the study of other properties of dehydrogenated dihydropyrimidines.

Experimental

Melting points were measured by an electro-thermal engineering micro-melting point apparatus and are uncorrected. NMR spectra were recorded on an INOVA 500 MHz instrument using DMSO-d_6. TLC was performed on GF254 silica gel plates (Yantai Huiyou Inc., China). Voltammetry and pH measurements were performed using a Selecta lab device model pHW300 Microprocessor. The catalyst was characterized using X-ray diffraction (XRD). Diffractograms were recorded on a Panalytical X'Pert PRO MPD diffractometer using Cu Kα irradiation (λ = 1.54059 Å). Scanning Electron Microscopy (SEM) was performed on a LEO 1430VP instrument. High-resolution transmission electron microscopy (HRTEM) was performed on a FEI TEC9G20 instrument. BET surface area analysis was performed using nitrogen sorption on a Micrometrics PHS-1020 accelerated surface area system. Samples were degassed at 200 °C for 12 h prior to experiments which were carried out at 77 K. The specific surface area of the material was determined by the BET method. All of the FT-IR and NMR spectra are available in the ESI.†

Catalyst preparation

Potassium containing OMS-2 (K-OMS-2) was synthesized using a variation of earlier reported procedures.[55,66–68] Briefly, to a solution of 59.0 mmol $MnSO_4 \cdot H_2O$ in 33 mL distilled water, 55.5 mmol of HNO_3 was added. The obtained solution was added dropwise to another solution consisting of 42.0 mmol $KMnO_4$ and 100 mL of distilled water, by using a dropping funnel, under vigorous stirring. The resulting grayish mixture was refluxed at 110 °C for 24 h, upon which the black precipitate was filtered, washed with distilled water until neutral, oven-dried at 120 °C overnight, and ground to fine powder.

This powder (5 g) was then dispersed in 75.0 mL of dry dichloromethane by means of a magnetic stirrer and while stirring at 700 rpm, chlorosulfonic acid (1.0 g, 8.55 mmol in 10.0 mL of CH_2Cl_2) was added dropwise over a period of 90 min at room temperature. The evolved HCl was eliminated by suction. Then the sulfonated OMS-2 was separated by sedimentation and washed several times with dichloromethane and dried under vacuum at 70 °C.

General procedure for the synthesis of benzo[4,5]imidazo[1,2-*a*]pyrimidines 5 or 2-amino-4-substituted-1,4-dihydrobenzo[4,5]imidazolo[1,2-*a*]pyrimidine-3-carbonitriles 6

A mixture of 2-aminobenzimidazole **3** (2 mmol), aldehyde **4** (2 mmol), acetylacetone **1** and OMS-2-SO_3H (35 mg, 0.1 mmol) in

water (2 mL) was heated to reflux for 45–90 min. Also, a mixture of 2-aminobenzimidazole **3** (2 mmol), aldehyde **4** (2 mmol), malononitrile **2** (2 mmol) and OMS-2-SO_3H (35 mg, 0.1 mmol) in water (2 mL) was heated to reflux for 10–30 min. After completion of the reaction (TLC), the solid was filtered off, washed with water and recrystallized from methanol (5 mL) to yield pure product **5** or **6**.

1-(4-Anthracen-9-yl-2-methyl-1,4-dihydro-benzo[4,5]imidazo [1,2-*a*]pyrimidin-3-yl)-ethanone (5a). Pale yellow powder, melting point: 277–279 °C; FT-IR (KBr): (ν_{max}/cm^{-1}); 3264 (NH), 2961, 2861 (CH), 1667, 1603, 1526 (conj. CN), 1442, 1377, 1252, 1208, 768; ^{1}H NMR (500 MHz, DMSO-d_6) δ_H: 10.11 (1H, brs, NH), 7.67 (1H, t, J = 8.0, ArH), 7.51–7.60 (9H, m, ArH), 7.29 (1H, t, J = 8.0, ArH), 7.08 (1H, t, J = 8.0, ArH), 6.77 (1H, d, J = 7.6, ArH), 6.41 (1H, s, CH), 2.51 (3H, s, Me), 2.18 (3H, s, COMe); ^{13}C NMR (100 MHz, DMSO-d_6) δ_C: 194.6, 146.7, 145.9, 142.8, 142.2, 141.4, 132.2, 130.5, 129.0, 128.3, 127.1, 124.0, 123.7, 123.5, 122.3, 121.3, 120.9, 119.4, 117.3, 110.5, 56.1, 31.3, 20.2.

1-[2-Methyl-4-(2-nitro-phenyl)-1,4-dihydro-benzo[4,5]imidazo[1,2-*a*]pyrimidin-3-yl]-ethanone (5b). Yellow powder, melting point: 280–282 °C; FT-IR (KBr): (ν_{max}/cm^{-1}); 3231 (NH), 3026, 2926 (CH), 1726 (conj. CO), 1660, 1608, 1564 (conj. CN), 1523 (conj. NO), 1458, 1384, 1354, 1273, 1134, 780, 737; ^{1}H NMR (500 MHz, DMSO-d_6) δ_H: 10.79 (1H, brs, NH), 8.45 (1H, d, J = 7.6, ArH), 8.21 (1H, d, J = 7.6, ArH), 7.83–7.91 (2H, m, ArH), 7.41 (1H, d, J = 8.0, ArH), 7.16 (1H, t, J = 7.6, ArH), 6.98 (1H, t, J = 7.2, ArH), 6.77 (1H, d, J = 8.0, ArH), 6.59 (1H, s, CH), 2.65 (3H, s, Me), 2.14 (3H, s, COMe); ^{13}C NMR (100 MHz, DMSO-d_6) δ_C: 194.3, 148.8, 145.8, 145.5, 142.3, 133.7, 131.7, 128.5, 121.7, 120.2, 119.3, 116.8, 113.8, 111.8, 110.1, 108.7, 55.1, 30.6, 19.7.

1-[4-(5-Bromo-2-hydroxy-phenyl)-2-methyl-1,4-dihydro-benzo[4,5]imidazo[1,2-*a*]pyrimidin-3-yl]-ethanone (5c). Pale yellow powder, melting point: 258–262 °C; FT-IR (KBr): (ν_{max}/cm^{-1}); 3423 (NH), 3326 (OH), 3089, 2924 (CH), 1756 (conj. CO), 1652, 1601, 1558 (conj. CN), 1469, 1381, 1275, 1118, 1056 (CBr), 1027 (CO), 862–818, 752; ^{1}H NMR (500 MHz, DMSO-d_6) δ_H: 10.67 (1H, brs, NH), 9.04 (1H, brs, OH), 7.28–7.39 (2H, m, ArH), 6.86–7.10 (3H, m, ArH), 6.56–6.63 (2H, m, ArH), 6.22 (1H, s, CH), 2.43 (3H, s, Me), 2.30 (3H, s, COMe); ^{13}C NMR (100 MHz, DMSO-d_6) δ_C: 193.9, 151.7, 146.5, 142.4, 140.8, 132.5, 131.5, 130.2, 129.0, 128.5, 127.4, 121.9, 120.3, 116.9, 109.9, 108.6, 54.9, 30.8, 19.9.

1-[4-(4-Hydroxy-3-methoxy-phenyl)-2-methyl-1,4-dihydro-benzo[4,5]imidazo[1,2-*a*]pyrimidin-3-yl]-ethanone (5d). Pale yellow powder, melting point: 273–275 °C; FT-IR (KBr): (ν_{max}/cm^{-1}); 3414 (OH), 3339 (NH), 2963, 2848 (CH), 1883 (conj. CO), 1674, 1591, 1514 (conj. CN), 1462, 1435, 1401, 1291, 1156, 1120 (CO), 1031, 867, 821, 783; ^{1}H NMR (500 MHz, DMSO-d_6) δ_H: 10.22 (1H, brs, NH), 8.56 (1H, brs, OH), 7.21–7.30 (2H, m, ArH), 6.58–6.70 (5H, m, ArH), 6.23 (1H, s, CH), 3.46 (3H, s, OMe), 2.30 (3H, s, Me), 2.07 (3H, s, COMe); ^{13}C NMR (100 MHz, DMSO-d_6) δ_C: 194.9, 148.9, 147.5, 146.3, 145.9, 142.8, 134.6, 132.1, 122.2, 120.6, 119.9, 117.4, 112.3, 111.9, 110.7, 109.0, 56.0, 55.9, 31.0, 20.1.

2-Amino-4-anthracen-9-yl-1,4-dihydro-benzo[4,5]imidazo [1,2-*a*]pyrimidine-3-carbonitrile (6a). Yellow powder, melting point: 239–243 °C; FT-IR (KBr): (ν_{max}/cm^{-1}); 3326 (NH), 3019, 2912 (CH), 2208 (triple CN), 1652, 1601, 1542 (conj. CN), 1446, 1262, 1172, 750; ^{1}H NMR (500 MHz, DMSO-d_6) δ_H: 10.82 (1H, brs, NH), 7.59 (1H, t, J = 8.0, ArH), 7.38 (1H, d, J = 7.6, ArH), 7.26 (1H, t, J = 7.2, ArH), 6.89–7.12 (9H, m, ArH), 6.58 (1H, d, J = 8.0, ArH), 6.23 (2H, s, NH_2), 5.20 (1H, s, CH); ^{13}C NMR (100 MHz, DMSO-d_6) δ_C: 152.0, 148.8, 143.9, 142.4, 131.3, 130.5, 129.1, 128.7, 127.9, 126.3, 125.2, 124.0, 123.7, 122.9, 122.4, 121.5, 120.8, 118.8, 117.5, 114.7, 57.2.

2-Amino-4-(2-nitro-phenyl)-1,4-dihydro-benzo[4,5]imidazo [1,2-*a*]pyrimidine-3-carbonitrile (6b). Yellow powder, melting point: 220–222 °C; FT-IR (KBr): (ν_{max}/cm^{-1}); 3398 (NH), 3132, 2929 (CH), 2192 (triple CN), 1677, 1600, 1569 (conj. CN), 1523 (conj. NO), 1470, 1348, 1286, 1126, 789, 745; ^{1}H NMR (500 MHz, DMSO-d_6) δ_H: 8.80 (1H, brs, NH), 7.97–8.01 (2H, m, ArH), 7.55 (1H, d, J = 7.6, ArH), 7.44 (1H, t, J = 8.0, ArH), 7.35 (1H, t, J = 8.0, ArH), 7.16–7.21 (2H, m, ArH), 7.02 (1H, d, J = 7.6, ArH), 6.32 (2H, s, NH_2), 5.61 (1H, s, CH); ^{13}C NMR (100 MHz, DMSO-d_6) δ_C: 151.6, 148.7, 141.2, 140.0, 139.1, 133.5, 131.0, 128.1, 127.3, 126.3, 125.8, 124.4, 121.1, 116.8, 114.4, 112.7, 56.3.

2-Amino-4-(5-bromo-2-hydroxy-phenyl)-1,4-dihydro-benzo [4,5]imidazo[1,2-*a*]pyrimidine-3-carbonitrile (6c). Yellow powder, melting point: 234–236 °C; FT-IR (KBr): (ν_{max}/cm^{-1}); 3383 (OH), 3256 (NH), 3186, 2929 (CH), 2198 (triple CN), 1647, 1599, 1472, 1271, 1120, 1072 (CBr), 1021 (CO), 862–815, 742; ^{1}H NMR (500 MHz, DMSO-d_6) δ_H: 8.60 (1H, brs, NH), 8.52 (1H, brs, OH), 7.57–7.68 (2H, m, ArH), 7.00–7.42 (5H, m, ArH), 6.85 (2H, s, NH_2), 5.25 (1H, s, CH); ^{13}C NMR (100 MHz, DMSO-d_6) δ_C: 152.2, 151.8, 148.7, 143.2, 132.6, 131.4, 129.7, 128.7, 128.1, 124.9, 121.4, 120.7, 117.6, 115.9, 114.2, 112.4, 56.1.

2-Amino-4-(4-hydroxy-3-methoxy-phenyl)-1,4-dihydro-benzo [4,5]imidazo[1,2-*a*]pyrimidine-3-carbonitrile (6d). Yellow powder, melting point: 222–226 °C; FT-IR (KBr): (ν_{max}/cm^{-1}); 3418 (OH), 3364 (NH), 3191, 2930 (CH), 2213 (triple CN), 1678, 1597, 1570 (conj. CN), 1468, 1321, 1275, 1127, 1075 (CO), 1025, 843–815, 738; ^{1}H NMR (500 MHz, DMSO-d_6) δ_H: 8.72 (1H, brs, NH), 8.61 (1H, brs, OH), 7.32–7.40 (2H, m, ArH), 7.13–7.25 (5H, m, ArH), 6.85 (2H, s, NH_2), 5.24 (1H, s, CH), 3.72 (3H, s, OMe); ^{13}C NMR (100 MHz, DMSO-d_6) δ_C: 151.8, 148.9, 144.2, 137.2, 135.9, 133.6, 130.0, 128.3, 124.7, 124.2, 121.6, 120.3, 118.8, 115.7, 112.5, 111.3, 57.2, 54.4.

General procedure for the oxidative dehydrogenation

2-aminobenzimidazole **3** (2 mmol), aldehyde **4** (2 mmol), acetylacetone **1** or malononitrile **2** (2 mmol), and OMS-2-SO_3H (35 mg, 0.1 mmol) in acetonitrile (2 mL) was heated to reflux until the disappearance of the starting reagents were complete (monitored by TLC). After completion of the first step, DDQ (1.2 mmol) solution in acetonitrile was added dropwise and slowly to the solution. This reaction was stirred for 1.5–2.5 h and gave a dark red precipitate. After completion of the oxidation step (indicated by TLC), the mixture was purified by short column chromatography (*n*-hexane/EtOAc, 10 : 4) to provide the desired products.

1-(4-Anthracen-9-yl-2-methyl-benzo[4,5]imidazo[1,2-*a*] pyrimidin-3-yl)-ethanone (7a). Dark red powder, melting point: 290–294 °C; FT-IR (KBr): (ν_{max}/cm^{-1}); 2922, 1650, 1537 (conj. CN), 1420, 1348, 1261, 1140, 752; ^{1}H NMR (500 MHz, DMSO-d_6)

δ_H: 7.57 (1H, t, J = 8.0, ArH), 7.47 (1H, d, J = 7.6, ArH), 7.21 (1H, t, J = 7.2, ArH), 6.94–7.17 (9H, m, ArH), 6.69 (1H, d, J = 8.0, ArH), 2.67 (3H, s, Me), 2.32 (3H, s, COMe); ^{13}C NMR (100 MHz, DMSO-d_6) δ_C: 196.2, 148.4, 146.9, 144.7, 143.9, 142.6, 136.5, 132.4, 130.2, 128.7, 127.6, 126.7, 125.4, 124.9, 123.7, 122.9, 121.5, 119.9, 118.4, 112.8, 60.2, 33.3, 20.8.

1-[2-Methyl-4-(2-nitro-phenyl)-benzo[4,5]imidazo[1,2-*a*] pyrimidin-3-yl]-ethanone (7b). Dark red powder, melting point: 293–295 °C; FT-IR (KBr): (ν_{max}/cm^{-1}); 1781 (conj. CO), 1650, 1551 (conj. CN), 1517 (conj. NO), 1430, 1410, 1347, 1298, 1112, 751, 744; ^{1}H NMR (500 MHz, DMSO-d_6) δ_H: 8.13–8.15 (1H, m, ArH), 7.75–7.78 (1H, m, ArH), 7.49 (1H, d, J = 7.6, ArH), 7.26 (1H, t, J = 8.0, ArH), 7.22 (1H, t, J = 8.0, ArH), 6.96–7.05 (2H, m, ArH), 6.63 (1H, d, J = 7.6, ArH), 2.76 (3H, s, Me), 2.27 (3H, s, COMe); ^{13}C NMR (100 MHz, DMSO-d_6) δ_C: 195.6, 149.7, 147.7, 146.8, 144.4, 135.8, 133.4, 131.7, 125.4, 122.7, 120.9, 118.9, 117.1, 113.2, 112.7, 109.4, 61.5, 32.4, 20.2.

1-[4-(5-Bromo-2-hydroxy-phenyl)-2-methyl-benzo[4,5]imidazo[1,2-*a*]pyrimidin-3-yl]-ethanone (7c). Dark red powder, melting point: 285–287 °C; FT-IR (KBr): (ν_{max}/cm^{-1}); 3397, 1731, 1650, 1520, 1451, 1376, 1261, 1112, 1041, 1012, 858–812, 749; ^{1}H NMR (500 MHz, DMSO-d_6) δ_H: 9.28 (1H, brs, OH), 7.50 (1H, d, J = 8.0, ArH), 7.15–7.23 (3H, m, ArH), 7.05 (1H, d, J = 8.0, ArH), 6.97 (1H, t, J = 7.6, ArH), 6.66 (1H, t, J = 7.6, ArH), 2.54 (3H, s, Me), 2.37 (3H, s, COMe); ^{13}C NMR (100 MHz, DMSO-d_6) δ_C: 194.8, 152.5, 147.8, 143.5, 141.4, 133.7, 132.9, 131.6, 130.4, 129.4, 128.4, 124.4, 121.7, 118.6, 110.2, 108.9, 62.1, 32.3, 20.1.

1-[4-(4-Hydroxy-3-methoxy-phenyl)-2-methyl-benzo[4,5]imidazo[1,2-*a*]pyrimidin-3-yl]-ethanone (7d). Dark red powder, melting point: 281–283 °C; FT-IR (KBr): (ν_{max}/cm^{-1}); 3416 (OH), 2960, 1727 (conj. CO), 1683, 1555 (conj. CN), 1450, 1418, 1273, 1209, 1076 (CO), 893–822, 747; ^{1}H NMR (500 MHz, DMSO-d_6) δ_H: 8.94 (1H, brs, OH), 7.30 (2H, dd J = 7.5, 3.6 Hz, ArH), 6.97–7.19 (3H, m, ArH), 6.55–6.68 (2H, m, ArH), 3.70 (3H, s, OMe), 2.42 (3H, s, Me), 2.20 (3H, s, COMe); ^{13}C NMR (100 MHz, DMSO-d_6) δ_C: 198.2, 152.8, 151.6, 149.9, 147.5, 143.2, 135.9, 133.5, 126.7, 122.7, 120.5, 118.6, 116.5, 112.2, 111.8, 110.0, 60.9, 55.9, 33.0, 20.9.

2-Amino-4-anthracen-9-yl-benzo[4,5]imidazo[1,2-*a*] pyrimidine-3-carbonitrile (8a). Dark red powder, melting point: 281–285 °C; FT-IR (KBr): (ν_{max}/cm^{-1}); 2928, 2209 (triple CN), 1649, 1536 (conj. CN), 1431, 1259, 1163, 744; ^{1}H NMR (500 MHz, DMSO-d_6) δ_H: 7.74 (1H, t, J = 8.0, ArH), 7.54–7.63 (9H, m, ArH), 7.27 (1H, t, J = 8.0, ArH), 7.00 (1H, t, J = 8.0, ArH), 6.65 (1H, d, J = 7.6, ArH), 6.28 (2H, s, NH_2); ^{13}C NMR (100 MHz, DMSO-d_6) δ_C: 153.4, 149.2, 145.8, 143.8, 132.2, 131.7, 130.1, 129.4, 128.5, 126.7, 125.1, 124.9, 123.2, 122.5, 121.9, 121.5, 120.8, 119.5, 118.5, 115.3, 62.3.

2-Amino-4-(2-nitro-phenyl)-benzo[4,5]imidazo[1,2-*a*] pyrimidine-3-carbonitrile (8b). Dark red powder, melting point: 276–278 °C; FT-IR (KBr): (ν_{max}/cm^{-1}); 2198 (triple CN), 1651, 1571 (conj. CN), 1512 (conj. NO), 1464, 1321, 1294, 1121, 769, 747; ^{1}H NMR (500 MHz, DMSO-d_6) δ_H: 8.50 (1H, d, J = 7.6, ArH), 8.29 (1H, d, J = 7.6, ArH), 7.86–7.98 (2H, m, ArH), 7.55 (1H, d, J = 8.0, ArH), 7.27 (1H, t, J = 7.6, ArH), 7.02 (1H, t, J = 7.2, ArH), 6.93 (1H, d, J = 8.0, ArH), 6.84 (2H, s, NH_2); ^{13}C NMR (100 MHz, DMSO-d_6) δ_C: 152.9, 149.2, 143.6, 141.5, 140.7, 135.7, 133.4, 130.5, 128.8, 127.5, 126.6, 125.7, 122.9, 118.8, 115.7, 113.4, 61.2.

2-Amino-4-(5-bromo-2-hydroxy-phenyl)-benzo[4,5]imidazo [1,2-*a*]pyrimidine-3-carbonitrile (8c). Dark red powder, melting point: 285–289 °C; FT-IR (KBr): (ν_{max}/cm^{-1}); 3372 (OH), 2206 (triple CN), 1654, 1461, 1264, 1118, 1059 (CBr), 1016 (CO), 859–813, 746; ^{1}H NMR (500 MHz, DMSO-d_6) δ_H: 8.71 (1H, brs, OH), 7.78 (1H, d, J = 7.8, ArH), 7.71 (1H, d, J = 7.8, ArH), 7.63 (1H, t, J = 7.2, ArH), 7.44–7.52 (2H, m, ArH), 7.23 (1H, s, ArH), 7.03 (1H, d, J = 7.6, ArH), 6.86 (2H, s, NH_2); ^{13}C NMR (100 MHz, DMSO-d_6) δ_C: 153.2, 152.7, 149.7, 144.6, 135.7, 133.6, 130.5, 129.4, 128.9, 126.7, 122.5, 120.9, 119.4, 116.8, 115.9, 113.7, 60.1.

2-Amino-4-(4-hydroxy-3-methoxy-phenyl)-benzo[4,5]imidazo [1,2-*a*]pyrimidine-3-carbonitrile (8d). Dark red powder, melting point: 284–288 °C; FT-IR (KBr): (ν_{max}/cm^{-1}); 3414 (OH), 2941, 2209 (triple CN), 1682, 1581 (conj. CN), 1461, 1318, 1261, 1118, 1112 (CO), 858–826, 731; ^{1}H NMR (500 MHz, DMSO-d_6) δ_H: 8.75 (1H, brs, OH), 7.68–7.77 (2H, m, ArH), 7.23–7.39 (3H, m, ArH), 6.91–7.00 (2H, m, ArH), 6.86 (2H, s, NH_2) 3.76 (3H, s, OMe); ^{13}C NMR (100 MHz, DMSO-d_6) δ_C: 153.6, 149.7, 145.3, 139.8, 136.2, 134.1, 131.9, 129.7, 125.7, 124.8, 122.4, 121.5, 119.8, 116.6, 113.7, 112.5, 60.9, 55.2.

Competition experiments

To prepare the solutions of metal ions, the chloride salts such as (Ca^{2+}, Fe^{3+}, Ni^{2+}, Cr^{3+}, Co^{2+}, Cu^{2+}, Zn^{2+}, Cd^{2+}, Mn^{2+}, Hg^{2+} and Sn^{2+}) were dissolved in acetonitrile to afford 1.25 × 10^{-4} M solutions. A 5 × 10^{-6} M solution of **7d** was prepared in acetonitrile. After mixing them for a few second, UV-vis spectra were taken at room temperature.

pH titration

Compound **7d** (0.87 mg, 0.0025 mmol) was dissolved in ethanol (8 mL), dilute alkali solution NH_4OH (0.01 M) was slowly added to the solution. After mixing them for a few minutes, UV-vis absorption spectra were taken at room temperature.

Conflicts of interest

There are no conflicts to declare.

Acknowledgements

Partial support of this study by Research Council of University of Guilan is gratefully acknowledged.

References

1 L. Ding, P. Rahimi, R. Hawkins, S. Bhatt and Y. Shi, *Appl. Catal., A*, 2009, **371**, 121–130.
2 J. Li, Q. Wang, Z. Guo, H. Ma, Y. Zhang, B. Wang, D. Bin and Q. Wei, *Sci. Rep.*, 2016, **6**, 23558.
3 P. T. Lieu, M. Heiskala, P. A. Peterson and Y. Yang, *Mol. Aspects Med.*, 2001, **22**, 1–87.
4 L. H. Yuen, R. M. Franzini, S. S. Tan and E. T. Kool, *J. Am. Chem. Soc.*, 2014, **136**, 14576–14582.

5 P. Bühlmann, E. Pretsch and E. Bakker, *Chem. Rev.*, 1998, **98**, 1593–1688.
6 N. Zhang, R. Qiao, J. Su, J. Yan, Z. Xie, Y. Qiao, X. Wang and J. Zhong, *Small*, 2017, **13**, 1604293.
7 D. Zhang, M. Zhang, Z. Liu, M. Yu, F. Li, T. Yi and C. Huang, *Tetrahedron Lett.*, 2006, **47**, 7093–7096.
8 K. K. Upadhyay, S. Upadhyay, K. Kumar and R. Prasad, *J. Mol. Struct.*, 2009, **927**, 60–68.
9 O. G. Nikolaeva, E. N. Shepelenko, K. S. Tikhomirova, Y. V. Revinskii, A. D. Dubonosov, V. A. Bren and V. I. Minkin, *Mendeleev Commun.*, 2016, **26**, 402–404.
10 Y.-T. Wang, S. Hu, Y. Zhang, H. Gong, R. Sun, W. Mao, D.-H. Wang and Y. Chen, *J. Photochem. Photobiol., A*, 2018, **355**, 101–108.
11 G. Dhaka, N. Kaur and J. Singh, *Supramol. Chem.*, 2015, **27**, 654–660.
12 A. Caballero, R. Martínez, V. Lloveras, I. Ratera, J. Vidal-Gancedo, K. Wurst, A. Tárraga, P. Molina and J. Veciana, *J. Am. Chem. Soc.*, 2005, **127**, 15666–15667.
13 T. Vamerali, M. Bandiera and G. Mosca, *Environ. Chem. Lett.*, 2010, **8**, 1–17.
14 J. B. Vincent, *Nutr. Rev.*, 2000, **58**, 67–72.
15 D. A. Eastmond, J. T. Macgregor and R. S. Slesinski, *Crit. Rev. Toxicol.*, 2008, **38**, 173–190.
16 R.-G. Lv, S.-W. Chen and Y. Gao, *Heterocycl. Commun.*, 2017, **23**, 389–394.
17 J. Kováčik, P. Babula, B. Klejdus and J. Hedbavny, *J. Agric. Food Chem.*, 2013, **61**, 7864–7873.
18 D. A. Brose and B. R. James, *Environ. Sci. Technol.*, 2010, **44**, 9438–9444.
19 A. K. Singh, V. K. Gupta and B. Gupta, *Anal. Chim. Acta*, 2007, **585**, 171–178.
20 K. Huang, H. Yang, Z. Zhou, M. Yu, F. Li, X. Gao, T. Yi and C. Huang, *Org. Lett.*, 2008, **10**, 2557–2560.
21 D. Liu, T. Pang, K. Ma, W. Jiang and X. Bao, *RSC Adv.*, 2014, **4**, 2563–2567.
22 Y. Lei, Y. Su and J. Huo, *J. Lumin.*, 2011, **131**, 2521–2527.
23 T. J. J. Müller, in *Functional Organic Materials*, 2006, ch. 5, pp. 179–223, DOI: 10.1002/9783527610266.
24 R. O. Rocha, M. O. Rodrigues and B. A. D. Neto, *ACS Omega*, 2020, **5**, 972–979.
25 L. Levi and T. J. J. Müller, *Chem. Soc. Rev.*, 2016, **45**, 2825–2846.
26 F. K. Merkt and T. J. J. Müller, *Isr. J. Chem.*, 2018, **58**, 889–900.
27 T. J. J. Müller, *Drug Discovery Today: Technol.*, 2018, **29**, 19–26.
28 D. Insuasty, J. Castillo, D. Becerra, H. Rojas and R. Abonia, *Molecules*, 2020, **25**, 505.
29 L. M. Ramos, M. O. Rodrigues and B. A. D. Neto, *Org. Biomol. Chem.*, 2019, **17**, 7260–7269.
30 P. S. G. Nunes, H. D. A. Vidal and A. G. Corrêa, *Org. Biomol. Chem.*, 2020, **18**, 7751–7773.
31 L. Cala, P. Villar, Á. R. de Lera, F. J. Fañanás, R. Álvarez and F. Rodríguez, *Chem. Sci.*, 2020, **11**, 9181–9190.
32 L. Zeng, B. Huang, Y. Shen and S. Cui, *Org. Lett.*, 2018, **20**, 3460–3464.
33 C. Oliver Kappe, *Tetrahedron*, 1993, **49**, 6937–6963.
34 N. Kaur, K. Kaur, T. Raj, G. Kaur, A. Singh, T. Aree, S.-J. Park, T.-J. Kim, N. Singh and D. O. Jang, *Tetrahedron*, 2015, **71**, 332–337.
35 C. O. Kappe, *Eur. J. Med. Chem.*, 2000, **35**, 1043–1052.
36 C. Oliver Kappe, W. M. F. Fabian and M. A. Semones, *Tetrahedron*, 1997, **53**, 2803–2816.
37 B. J. Broughton, P. Chaplen, P. Knowles, E. Lunt, S. M. Marshall, D. L. Pain and K. R. H. Wooldridge, *J. Med. Chem.*, 1975, **18**, 1117–1122.
38 A. A.-m. Abdel-hafez, *Arch. Pharmacal Res.*, 2007, **30**, 678.
39 J. J. Nunes, X. Zhu, P. Amouzegh, C. Ghiron, D. N. Johnson and E. C. Power, *US Pat.*, US7504396B2, 2009.
40 J. J. Nunes, X. T. Zhu, P. Amouzegh, C. Ghiron, D. N. Johnston and E. C. Power, WO Pat., 005009443, 2005.
41 M. Cheung, P. A. Harris, M. Hasegawa, S. Ida, K. Kano, N. Nishigaki, H. Sato, J. M. Veal, Y. Washio and R. I. West, WO Pat., 2002044156, 2002.
42 J. Yuan, K. Laubernds, Q. Zhang and S. L. Suib, *J. Am. Chem. Soc.*, 2003, **125**, 4966–4967.
43 Y. Wang, X. Meng, G. Chen and P. Zhao, *Catal. Commun.*, 2018, **104**, 106–111.
44 X. Meng, Y. Wang, Y. Wang, B. Chen, Z. Jing, G. Chen and P. Zhao, *J. Org. Chem.*, 2017, **82**, 6922–6931.
45 S. L. Suib, *Acc. Chem. Res.*, 2008, **41**, 479–487.
46 M. Bibes and A. Barthelemy, *IEEE Trans. Electron Devices*, 2007, **54**, 1003–1023.
47 D. M. D'Alessandro and F. R. Keene, *Chem. Soc. Rev.*, 2006, **35**, 424–440.
48 K. Ragavendran, D. Vasudevan, A. Veluchamy and B. Emmanuel, *J. Phys. Chem. B*, 2004, **108**, 16899–16903.
49 S. L. Suib, *J. Mater. Chem.*, 2008, **18**, 1623–1631.
50 L. Yun, Y. Li, C. Zhou, L. Lan, M. Zeng, M. Mao, H. Liu and X. Zhao, *Appl. Catal., A*, 2017, **530**, 1–11.
51 Z. Sihaib, F. Puleo, J. M. Garcia-Vargas, L. Retailleau, C. Descorme, L. F. Liotta, J. L. Valverde, S. Gil and A. Giroir-Fendler, *Appl. Catal., B*, 2017, **209**, 689–700.
52 F. Mardani, A. Khorshidi and S. Gholampoor, *ChemistrySelect*, 2019, **4**, 8015–8020.
53 A. Khorshidi and S. Shariati, *Chin. J. Catal.*, 2015, **36**, 778–784.
54 A. Khorshidi, S. Shariati and M. Abootalebi, *J. Serb. Chem. Soc.*, 2016, **81**, 1069–1079.
55 N. N. Opembe, C. K. King'ondu and S. L. Suib, *Catal. Lett.*, 2012, **142**, 427–432.
56 R. K. Ali and B. Fahimeh, *Lett. Org. Chem.*, 2011, **8**, 631–636.
57 M. V. Reddy, J. Oh and Y. T. Jeong, *C. R. Chim.*, 2014, **17**, 484–489.
58 B. Insuasty, A. Salcedo, A. Rodrigo, J. Quiroga, M. Nogueras and A. Sánchez, *Heterocycl. Commun.*, 2002, **8**, 287–292.
59 H. Sheibani and M. Babaie, *Russ. Chem. Bull.*, 2013, **62**, 2202–2208.
60 J. Liu, M. Lei and L. Hu, *Green Chem.*, 2012, **14**, 840–846.
61 L. Seyedakbari, G. M. Ziarani, A. Badiei, M. Yadavi, P. Hajiabbasi and A. A. Soorkic, *Res. Chem. Intermed.*, 2013, **64**, 832–837.

62 M. Abedini, F. Shirini, M. Mousapour and O. Goli Jolodar, *Res. Chem. Intermed.*, 2016, **42**, 6221–6229.
63 H. R. Shaterian, N. Fahimi and K. Azizi, *Res. Chem. Intermed.*, 2014, **40**, 1879–1898.
64 C.-S. Yao, S. Lei, C.-H. Wang, C.-X. Yu, Q.-Q. Shao and S.-J. Tu, *Chin. J. Chem.*, 2008, **26**, 2107–2111.
65 A. G. Püntener, R. Pedrazzi, T. Clausen, Klaus Hunger, W. Bauer, M. Filosa and E. Ross, in *Industrial Dyes Chemistry, Properties, Applications*, ed. Klaus Hunger, Wiley–VCH Verlag GmbH & Co. KGaA, Weinheim, Germany, 1st edn 2002, ch. 5, pp. 427–541, DOI: 10.1002/3527602011.
66 N. N. Opembe, Y.-C. Son, T. Sriskandakumar and S. L. Suib, *ChemSusChem*, 2008, **1**, 182–185.
67 Y.-F. Shen, R. P. Zerger, S. L. Suib, L. McCurdy, D. I. Potter and C.-L. O'Young, *J. Chem. Soc., Chem. Commun.*, 1992, 1213–1214, DOI: 10.1039/C39920001213.
68 N. N. Opembe, C. K. King'ondu, A. E. Espinal, C.-H. Chen, E. K. Nyutu, V. M. Crisostomo and S. L. Suib, *J. Phys. Chem. C*, 2010, **114**, 14417–14426.